crystals

MDPI

Article

Study of Microstructure and Properties of AZ91 Magnesium Alloy Welded Joint with Magnetic Field and TiO_2 Activated Flux

Guiqing Zhang *, Xintong Liu and Yunhai Su

School of Materials Science and Engineering, Shenyang University of Technology, Shenyang 110870, China
* Correspondence: zgq2060@163.com; Tel.: +86-139-9814-5109

Abstract: In order to improve the weldability and bearing capacity of AZ91 magnesium alloy welded joints, magnetic field and active flux were added in the TIG welding process. In the welding process, the magnetic field and welding parameters were unchanged, and the coating amount of active flux was adjusted. The formability, mechanical properties, and microstructure of the welded joints under different coating amounts of activated flux were analyzed, and the crystallization nucleation characteristics of molten pool were discussed. The experimental results reveal that the combined effect of the magnetic field and activated flux has a significant effect on increasing the penetration and promoting mechanical properties. When the coating amount of activated flux is 3 mg/cm^2, the highest penetration of the welded joint is obtained, which is 141% of that without activated flux. Meanwhile, the mechanical properties reach the maximum, which is a tensile strength of 292 MPa, elongation of 11.2%, and weld zone hardness of 75.6 HV (0.5 Kgf). The combined effect of TiO_2 flux and magnetic field does not change the phase composition and the grain orientation of a weld metal but can affect the grain size. The average grain size of a weld metal under an activated flux coating amount of 3 mg/cm^2 is 18.2% smaller than that under an activated flux coating amount of 1 mg/cm^2.

Keywords: TiO_2-activated flux; longitudinal alternating magnetic field; AZ91 magnesium alloy; microstructure and properties

Citation: Zhang, G.; Liu, X.; Su, Y. Study of Microstructure and Properties of AZ91 Magnesium Alloy Welded Joint with Magnetic Field and TiO_2 Activated Flux. *Crystals* **2022**, *12*, 1135. https://doi.org/10.3390/cryst12081135

Academic Editor: Cyril Cayron

Received: 29 July 2022
Accepted: 8 August 2022
Published: 12 August 2022

1. Introduction

Magnesium alloys are widely used in aerospace, automobile industry, and 3C products because of their advantages, such as low density, high specific strength, excellent damping capacity, and easy recovery [1,2]. Due to the characteristics of magnesium alloys, such as low melting point, low viscosity, and high chemical activity, many defects can form easily during the welding process, including slag, cracks, and porosities. In order to ensure the welding quality, lots of welding technologies for magnesium alloys have been studied, including tungsten inert gas (TIG) arc welding [3–5], metal inert gas (MIG) arc welding [6,7], friction stir welding (FSW) [8,9], resistance spot welding (RSW) [10,11], laser beam welding (LBW) [12,13], etc. Commonly used technologies were TIG and MIG welding. TIG welding has become the main technology used for welding magnesium alloys due to the small deformation of welded joint, narrow heat-affected zone, and high mechanical properties. However, because the arc is free and the current density of the arc is limited by the diameter of tungsten electrode, the TIG welding itself has some limitations, such as heat loss, small arc force, and low energy density. Therefore, the penetration of single-pass welding is shallow, which makes the welding efficiency low. Aiming to solve this problem, lots of pieces of research have been done. The activated tungsten insert gas (A-TIG) welding process was developed by the Paton Electric Welding Institute in the 1960s. In this process, activated flux was applied to the plate surface before welding, and an increase in penetration was achieved. Due to a wide range of components, rich sources, low prices, and good economic benefits of activated flux, lots of research on A-TIG has been carried out and promote the development of A-TIG welding technology [14–18].

The research on A-TIG welding has been carried out in China since the 1990s. Many studies about magnesium alloys were accomplished. The initial research committed to developing activated flux, which could increase the penetration obviously. The effect of metal-activated fluxes, oxide-activated fluxes, chloride-activated fluxes, fluoride-activated fluxes, and compound-activated fluxes on the weld penetration of magnesium alloy have been reported [19–24]. The research results showed that oxide- and chloride-activated flux could effectively increase weld penetration and make weld formation good. Although the mechanism was not unified, it is generally believed that the action mechanism of oxide-activated flux is mainly the interaction between activated flux and molten pool. The mechanism of chloride-activated flux is mainly the interaction between activated flux and arc. Although A-TIG welding has an obvious effect on increasing weld penetration and welding efficiency, it has a limited effect on refining microstructure and improving the performance of weld joints. Zhang et al. [19] found that the activated flux made grains of weld metal coarsen as compared to that without activated flux. The same conclusion was deduced by Shen et al. [25]. Qin et al. [26] reported the effect of welding current on AZ61/ZK60 dissimilar magnesium alloy in TIG and A-TIG welding. It was found that the grain size of the fusion zone of TIG and A-TIG welding could be refined and the tensile strength increased under the optimal current. But the grain size of A-TIG welding was not significantly different from that of TIG welding, and the tensile strength was lower than that of TIG welding. So, it can be seen that the activated flux has a positive effect on improving welding efficiency, but its effect on improving comprehensive mechanical properties of the welded joint is limited.

It is well known that the welding process under the action of magnetic field has attracted more and more attention, due to its advantages of its simple process, low cost, low energy consumption, and grain refinement. As the obvious effect on refining microstructure and improving mechanical properties, the longitudinal alternating magnetic field was mostly applied in the welding process [27–33]. Previous studies [34–37] have shown that the introduction of the magnetic field during welding can change the mass and heat transfer process of liquid metal in the molten pool, which can refine grains and improve properties of magnesium alloy welded joints.

Therefore, the application of a magnetic field to the magnesium alloy A-TIG welding may play a complementary role, which not only can remain the higher weld penetration but also can refine the grains and improve the performance of welded joints. This is of great practical significance for the application of magnesium alloys. Thus, in the present study, a longitudinal alternating magnetic field was applied in the A-TIG welding process of magnesium alloy. The activated flux was selected as TiO_2. During the test, the amount of activated flux coating was variable. The formability, microstructure, phase composition, grain orientation, and mechanical properties of welded joints were systematically investigated to reveal the role of the magnetic field and activated flux playing in the magnesium alloy welding.

2. Materials and Methods

Commercial hot-rolled AZ91 magnesium alloy plates with a dimension of 100 mm × 100 mm × 5 mm were selected as the base metal. The chemical composition of the base metal is given in Table 1.

Table 1. Chemical composition of the base metal (wt%).

Al	Zn	Mn	Si	Cu	Fe	Mg
8.3–9.7	0.35–1	0.15–0.5	<0.01	<0.03	<0.005	Balance

Before this experiment, orthogonal experiments were used to optimize the parameters, including welding current, excitation current, and excitation frequency, and the optimized value is 80 A, 1.5 A, 30 H_Z, respectively. Thus, in the experiment, only the coating amount of

activated flux was adjusted. Before welding, the surface of plates were polished to remove the contaminants and oxide. TiO_2-activated flux in powdered form was mixed with a carrier solvent of ethanol to make a fine paste, and uniformly applied to the surface of plates with a brush. The coating amount of activated flux was 1 mg/cm^2, 2 mg/cm^2, 3 mg/cm^2, 4 mg/cm^2, 5 mg/cm^2, respectively. The coated plates were placed under room temperature for 24 h until the moisture and alcohol was completely evaporated, and then welded by WSE-50 inverter welding machine. The longitudinal magnetic field was generated by the excitation coil placed on the welding torch, shown in Figure 1. Welding parameters are as follows: welding speed is 300 mm/min, extension of tungsten is 2 mm, arc length is 2 mm~4 mm, Argon gas flow rate is 10–15 L/min. For comparison, the welded joints were also prepared at the same welding parameters mentioned above without applying magnetic field.

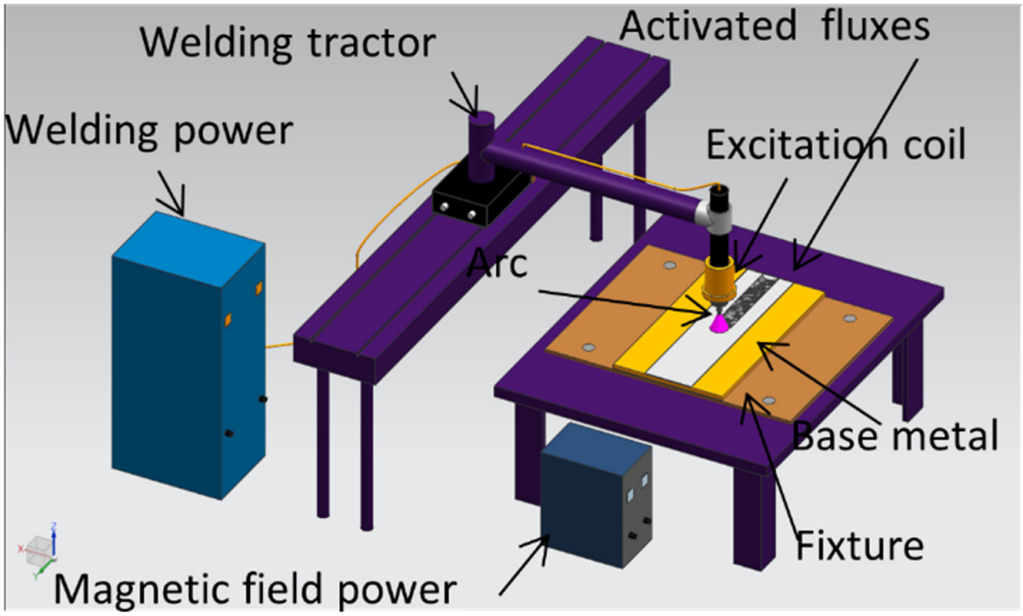

Figure 1. Schematic diagram of welding device.

After welding, the specimens were cross-sectioned from the welded plates and fine polished for microstructure and mechanical properties of welded joints. The weld penetration and width were measured using body vision microscope. The microstructure was observed by scanning electron microscopy (Hitachi S-3400, Hitachi microscopes, Tokyo, Japan). XRD-700 was used to determine the phases formed in the weld metal. The grain size and orientation of welded joints were characterized by EBSD (ZEISS G300, ZEISS, Oberkochen, Germany). The length, width, and thickness directions of the specimens were defined as the rolling direction (RD), transverse direction (TD), and normal direction (ND), respectively, shown in Figure 2. The EBSD specimens were ground and polished first, and then mechanically polished until the surfaces were bright and without visible scratches under the optical microscope. Final electrolytic polishing was performed using the solution mixed with 10% perchloric acid and 90% alcohol. The temperature of electrolyte is controlled at −30 °C. The electrolytic voltage and time is 15 V and 120 s, respectively. Microhardness was determined with THVS-5 Vickers hardness tester under a dwell time of 15 s with a load of 500 g. The tensile tests were carried out using a universal testing machine under a velocity of 3 mm/min.

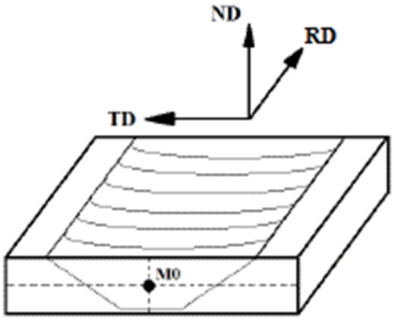

Figure 2. EBSD sampling diagram.

3. Results and Discussion

3.1. Formation of the Welded Joints

The formation of the A-TIG welded joints with and without magnetic field are shown in Figure 3. It can be seen from Figure 3a that all penetration of the welded joints with activated flux are higher than that without activated flux. This indicates that A-TIG welding can significantly increase the weld penetration than traditional TIG welding, no matter whether the magnetic field is applied or not. The weld penetration and width both increase first and then decrease with the increase in activated flux coating amount, but the activated flux coating amount corresponding to their maximum value is not consistent. The introduction of a magnetic field does not change the above change law. For weld penetration, the maximum weld penetration is obtained when the activated flux coating amount is 3 mg/cm^2, and the weld penetration with magnetic field is larger than that without magnetic field. For weld width, the maximum weld width is obtained when the activated flux coating amount is 2 mg/cm^2, and the weld penetration without a magnetic field is larger than that with a magnetic field. Whether with a magnetic field or without a magnetic field, the forming factor of weld decreases gradually with an increase in activated flux coating amount. However, under the condition of the magnetic field, the forming factor fluctuates in the process of decreasing. This shows that although the applied magnetic field does not change the action trend of the activated flux, it still has a significant influence on the welding process. In order to further compare the weld forming status under TIG, A-TIG and M+A-TIG, the corresponding data are summarized, as shown in Figure 3b. In the state of A-TIG and M+A-TIG, the coating amount of activated flux is 3 mg/cm^2. It is obvious that the highest penetration and the smallest forming factor are obtained under M+A-TIG; these are beneficial for improving welding efficiency.

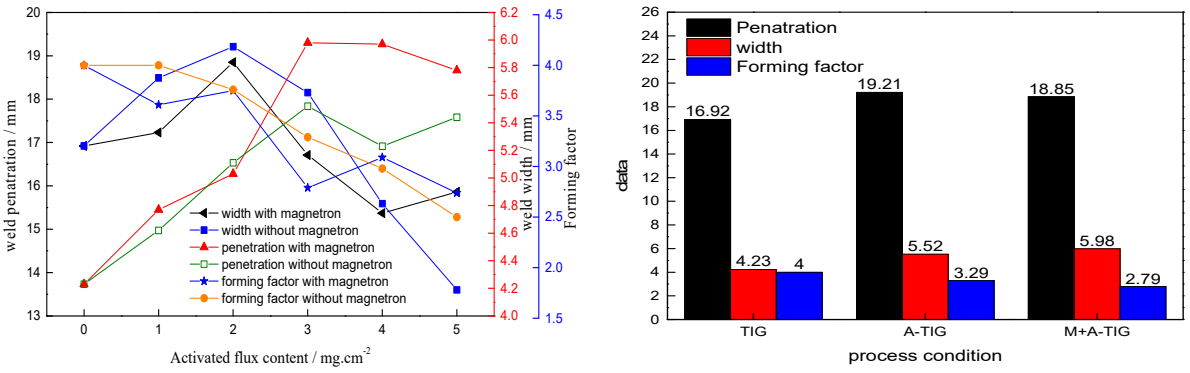

(**a**) (**b**)

Figure 3. Formation of the joints with and without magnetic field. (**a**) Under different flux coating amounts; (**b**) Under different process.

3.2. Microstructure of Welded Joints

The weld metal with and without applied magnetic field at 3 mg/cm^2 activated flux coating amount are selected for microstructure and XRD analysis. The results are shown in Figure 4. As shown in Figure 4a,b, both of the weld metal are composed of dark gray primary phase and second phase distributed in gray-white grain boundary, the second phase particles exhibit a diffuse distribution. It can be seen from Figure 5 that the phase composition of weld metal does not change with or without applied magnetic field. It contains α-Mg, $Al_{12}Mg_{17}$, MgO and TiO. The α-Mg is the matrix and $Al_{12}Mg_{17}$ is the second phase, MgO and TiO are the inclusions. Normally, TiO should not be present in magnesium alloys, but TiO was detected in the samples of XRD test. This can be ascribed to the reaction between TiO_2 flux and matrix Mg under the action of the high temperature of the arc that generated MgO and TiO. These generated substances were involved in the molten pool under the action of the arc and did not float out of molten pool in time during the subsequent solidification and stayed in the weld metal. As seen from the XRD diffraction pattern, the application of the magnetic field does not change the distribution of diffraction peaks. For the matrix α-Mg, the strongest diffraction peaks are both obtained on the (101) crystal plane, which indicates that the application of the magnetic field shows no influence on the crystal orientation at the same coating amount but has an obvious enhancement effect on the diffraction peak of (002) crystal plane.

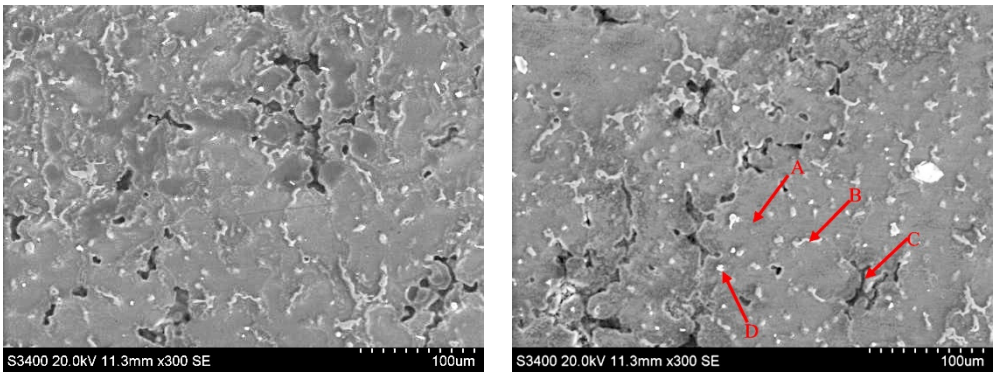

(**a**) (**b**)

Figure 4. SEM images and XRD results of weld metal under flux coating amount of 3 mg/cm^2. (**a**) SEM image of applying no magnetic field; (**b**) SEM image of exerting magnetic field.

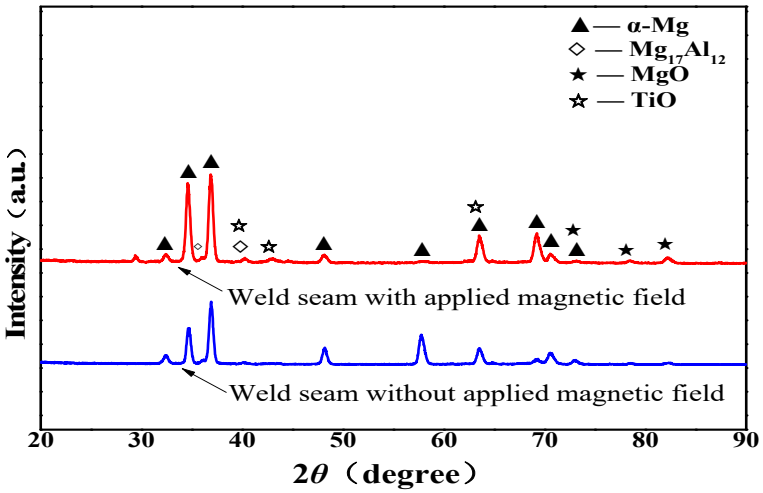

Figure 5. XRD results with and without magnetic field.

The phase composition of weld metal with and without magnetic field shows no difference, so only the weld metal with the magnetic field is selected for EDS analysis to identify the element distribution. Four sites located at 'A', 'B', 'C', 'D' in Figure 4b (as marked by red arrow) were analyzed. The site A is the area containing a primary crystal, site B is the gray-white area of a grain boundary, site C is the gray-black area of a grain boundary, and site D is the area containing a white, bright substance. The results are shown in Figure 5. It can be observed that two chemical elements (Mg, Al) are contained in site A and site C, and four chemical elements (Mg, Al, Zn/Ti) are contained in site B and site D. According to the binary alloy phase diagram of Mg-Al, the eutectic reaction of Mg-Al occurs at 437 °C, forming α-Mg and β/γ phases. In equilibrium, the solubility of Al in Mg is 11.5 wt% at high temperature and 1.5 wt% at room temperature. Since the welding process is a kind of rapid heating and cooling, the solidification process of a molten pool metal is non-equilibrium solidification crystallization; its composition deviates from the equilibrium composition. As shown in Figure 6a, site A consists of 97.77 wt% Mg and 2.23 wt% Al, suggesting that it is α-Mg. Site B is composed of 94.73 wt% Mg, 4.67 wt% Al and 0.6 wt% Zn; it is considered as a mixture of α-Mg and $Mg_{17}Al_{12}$ (with a higher solid solution of Zn). It is inferred that site C is a mixture of α-Mg and $Mg_{17}Al_{12}$ judging from the chemical contents. Site D contains Mg, Al, and Ti elements; according to the XRD results shown in Figure 6c, it can be concluded that it is corresponding to α-Mg and TiO.

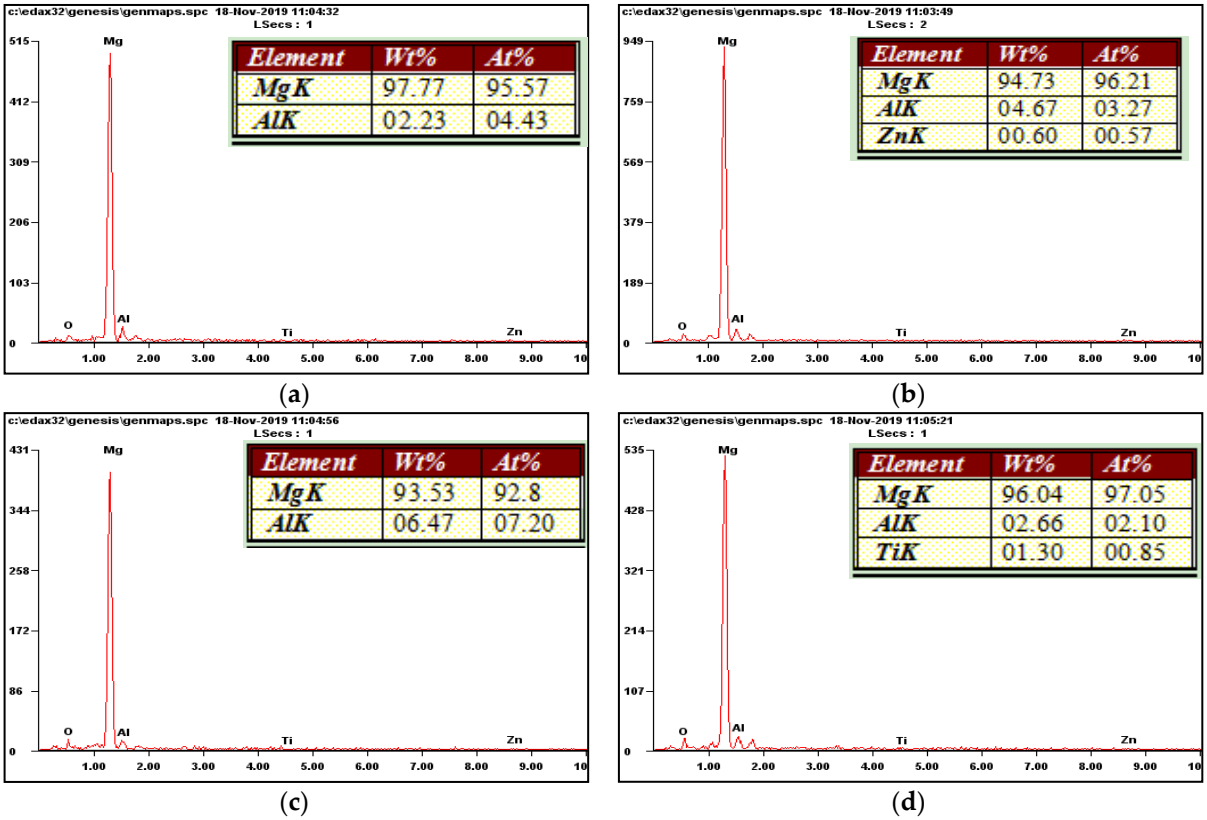

Figure 6. EDS analysis results of weld metal when applying magnetic field. (**a**) Site A; (**b**) Site B; (**c**) Site C; (**d**) Site D.

3.3. Change of Grain Size and Orientation of Weld Metal with and without Magnetic Field

The EBSD maps and grain size in weld metal with and without magnetic field at 3 mg/cm^2 activated flux coating amount are shown in Figure 7b,c,e,f. The same test was carried on base metal (BM) for comparison, the results are shown in Figure 7a,d.

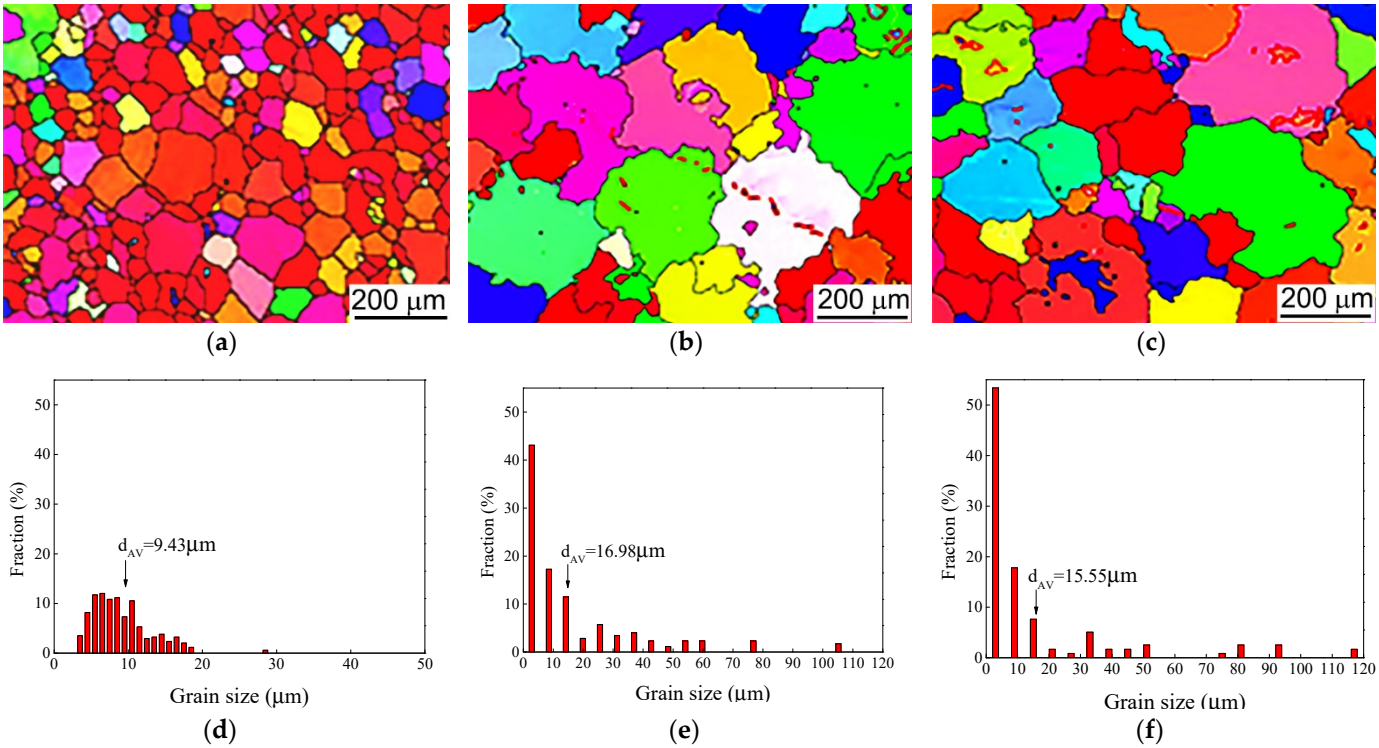

Figure 7. EBSD maps and grain size. (**a**,**d**) BM; (**b**,**e**) weld metal without magnetic field at 3 mg/cm^2; (**c**,**f**) weld metal with magnetic field at 3 mg/cm^2.

As shown in Figure 7, the particles of BM are finer than that of weld metal with or without magnetic field. The grain size in BM is 9.43 μm, while it is 16.98 μm and 15.55 μm without and with magnetic field, respectively. It should be noted that the average grain size of weld metal with magnetic field is smaller than that without magnetic field, which is due to the combined effects of activated flux and magnetic field. For one thing, TiO_2-activated flux will change the surface tension gradient of molten pool from negative to positive [36]. This will change the flow direction of the liquid molten pool, and finally the flow mode of the liquid molten pool will change from center to periphery to periphery to center. This change of flow mode in a molten pool has a good effect on increasing weld penetration but has no obvious effect on the microstructure of weld metal. Therefore, the grain size of weld metal is slightly larger than that of base metal. For another, the applied magnetic field can act on the arc to cause it rotate under the Lorentz force [37]. The rotating arc will drive the molten pool to rotate accordingly, but it has a certain lag. Since the flow mode of molten pool has been changed from the periphery to the center by TiO_2-activated flux, the liquid molten pool will move downward spirally under the combined action of the magnetic field and TiO_2-activated flux. This will make the scouring effect of liquid metal on the crystallization front near the fusion line more obvious. The primary or secondary dendrite arms of columnar crystals formed, due to a large temperature gradient in the initial stage of crystallization, will be subject to a large shear force. When the shear force reaches a certain level, the dendrite arms will be broken and dissolve into the moving molten pool, part of which will be remelted to participate in the solidification and solute redistribution of molten pool, part of which, unmelted, will be preserved in the form of a second phase and exist as a heterogeneous nucleation source to play a role in refining grains. This is the reason for the grain refinement of the weld metal with magnetic field and activated flux, compared with that without magnetic field.

The pole figures of three samples corresponding to Figure 7a–c are shown in Figure 8. The supply state of AZ91 magnesium alloy used in the test is rolled state, it would form a basal texture with a (0001) plane parallel to the rolling plane. Therefore, as shown in Figure 8a, the crystal in BM shows a tendency of preferential growth on the (0001) crystal

plane. When the TiO_2 activated flux acts alone or in conjunction with the magnetic field on the welding process, It can be observed from Figure 8b,c that the pole density distributes randomly, indicating that there is no crystal orientation behavior on the crystal planes. These are mainly caused by the change in flow mode of the molten pool. Under the combined action of two driving forces, the liquid metal will spiral downward (shown in Figure 7), which makes the movement of the molten pool more violent and the solute redistribution more uniform, thereby inhibiting the emergence of preferential growth behavior.

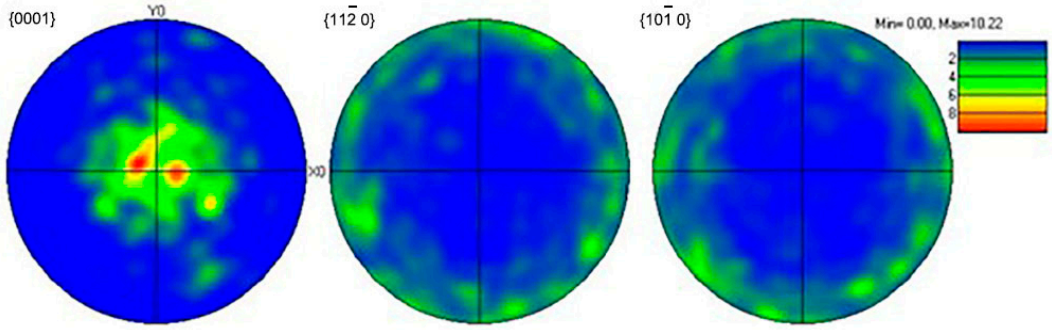

(**a**)

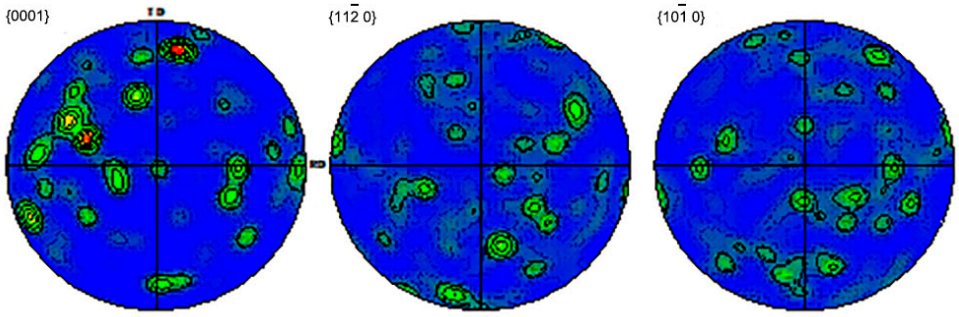

(**b**)

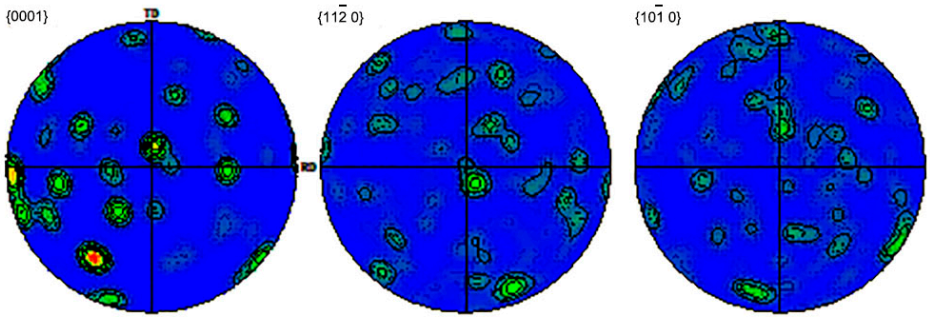

(**c**)

Figure 8. Pole figures of BM (**a**), weld metal at 3 mg/cm^2 without magnetic field (**b**), and weld metal at 3 mg/cm^2 with magnetic field (**c**).

3.4. Change of Grain Size and Orientation of Weld Metal with Magnetic Field at Different Activated Flux Coating Amounts

In order to compare the grain growth mode and grain size change law of weld metal under different activated flux amounts with magnetic field, EBSD is used to detect it, and the results are shown in Figure 9. From the crystal orientation diagram and reverse pole diagram, it can be found that the crystal orientation growth behavior of weld metal

is not obvious under different amounts of activated flux. This is mainly because under the combined action of external magnetic field and activated flux, the liquid molten pool presents spiral downward rotation. The movement mode of molten pool will affect the crystallization and nucleation characteristics of crystals during solidification. The composition gradient and temperature gradient of the crystal front are reduced, and the preferred growth mode is inhibited. This will promote the formation of equiaxed crystals and reduce the anisotropy of weld metal. Therefore, it has a good effect on improving the crack resistance and comprehensive mechanical properties of a welded joint. Although the increase in activated flux coating amounts has no obvious effect on the preferred growth behavior of weld metal, it still has a great influence on the grain size. As can be seen from Figure 9b,d,f, with the increase in activated flux amount, the grain size of weld metal first decreases and then increases. When the amount of activated flux is 3 mg/cm^2, the average grain size of the weld metal reaches the minimum value of 15.55 µm. According to the basic principle of metalology, the smaller the grain size of material, the larger the corresponding grain boundary area. The increase in grain boundary area will increase the deformation resistance of material in the process of deformation and then improve its bearing capacity. Therefore, when the amount of activated flux is 3 mg/cm^2, the grain boundary of weld metal is the most, which is very beneficial to improve the mechanical properties of weld metal. The correlation law can be confirmed in the subsequent mechanical property data.

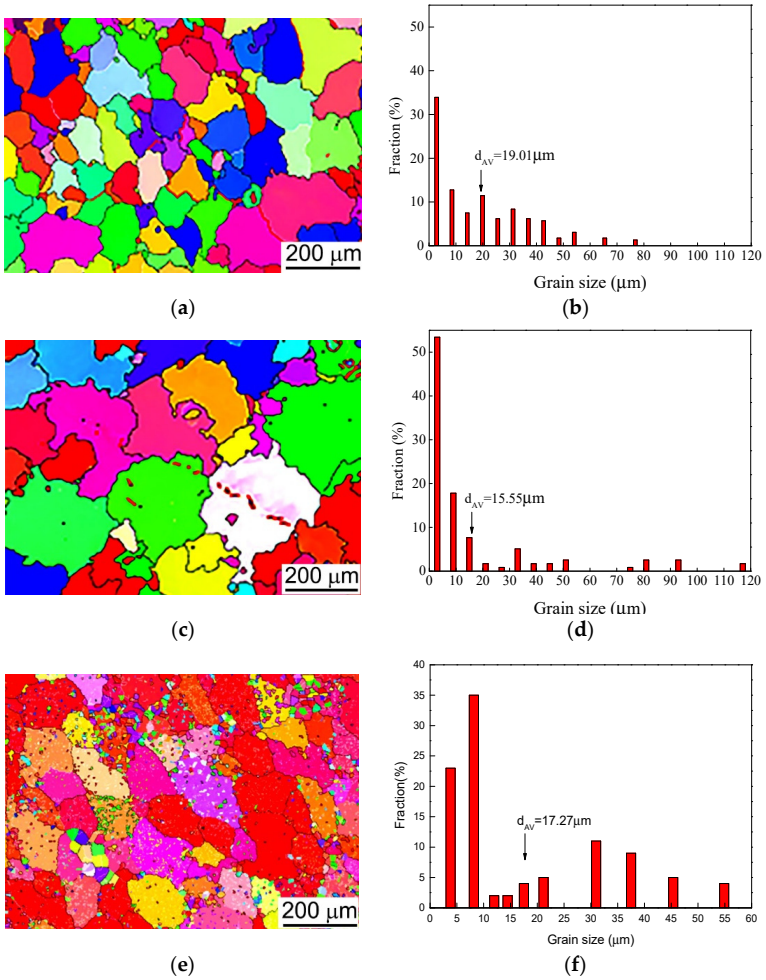

Figure 9. EBSD maps and grain size of weld metal with magnetic field. (**a**,**b**) 1 mg/cm^2; (**c**,**d**) 3 mg/cm^2; (**e**,**f**) 5 mg/cm^2.

3.5. Mechanical Properties of Welded Joins

Figure 10 shows the hardness of weld metal at different activated flux coating amounts and BM. It can be seen that the hardness increases at first and then decreases with the increase in activated flux coating amount and reaches the maximum at 3 mg/cm^2 (75.6 HV, 78.9 HV, respectively). Applying with or without the magnetic field, the hardness of the weld metal under each activated flux coating amount is higher than that of the BM. The hardness variation is mainly related to the grain size and the size and distribution of the second phase particulars. But as shown in Figure 7, the average grain size of the weld metal applied with and without magnetic field at an activated flux coating amount of 3 mg/cm^2 (with the maximum hardness, respectively) is larger than that of the BM. Therefore, their increased hardness can be attributed to the second phase enhancement of $Al_{12}Mg_{17}$. As shown in Figure 5a,b, many fine $Al_{12}Mg_{17}$ particulars are precipitated at the grain boundaries and diffusely distributed. Moreover, by comparing the two curves, it can be found that the hardness of the weld metal under magnetic field is lower than that without magnetic field, but the difference between the two is small. This phenomenon is inconsistent with the change law of grain size in weld metal. Generally speaking, the increase in hardness depends not only on the grain size but also on the number and distribution of the second phase and the spacing of the secondary dendrite arms. In this paper, the grain size is mainly measured because the number and distribution of the second phase are almost the same. The secondary dendrite spacing is also the same. Under normal circumstances, the smaller the grain size of the material, the better its macro mechanical properties should be. This situation in this experiment is mainly due to the difference of test points in the process of hardness testing.

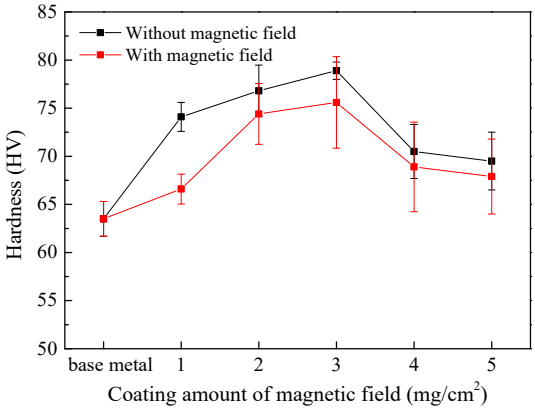

Figure 10. Hardness of weld metal and BM.

Figure 11 shows the tensile properties of welded joints and BM. As shown in Figure 11a, the tensile strength of welded joins presents a positive correlation with the coating amount of activated flux until it arrives to 3 mg/cm^2, the tensile strength decreases afterwards. The maximum value is obtained at 3 mg/cm^2, which is 292 MPa, 14% higher than that no magnetic field. This value is basically equivalent to the tensile strength of the BM. As shown in Figure 11b, it can be seen that, with increase in activated flux amount, the elongation shows an increasing trend up to their maximum (11.2% and 8.75%, with and without magnetic field, respectively). The elongation shows a downward trend. The overall increase in tensile strength and elongation manifests that the applied magnetic field has a significant effect on improving the tensile properties of welded joints. On the one hand, the applied magnetic field stirs the molten pool, which makes the movement of the molten pool more violent, the solute distribution more uniform, and the crystal grains effectively refined. The grain refinement implies that more grain boundaries are formed and become the main resistance to dislocation movement during the plastic deformation. Grain boundaries will be transformed into tearing edges during stretching. These tearing edges can be found in the fracture morphology in Figure 12. From the fracture morphology,

there is little difference in tensile fracture under different amounts of activated flux. The number of dimples is relatively small, and small cleavage surfaces appear locally, indicating that the plasticity of these welded joint is relatively poor. Moreover, the fine and scattered second-phase particles pin the grain boundaries and improve the strength of welded joints. On the other hand, after the introduction of magnetic field and activated flux, the texture of weld metal disappears and its plastic deformation ability at room temperature is improved. Under the action of grain refinement, second phase strengthening and weakening texture, the welded joint with magnetic field shows better tensile properties under each coating amount. When the activated flux coating amount is 3 mg/cm^2, the tensile strength and elongation of welded joints reach the performance level of the base material.

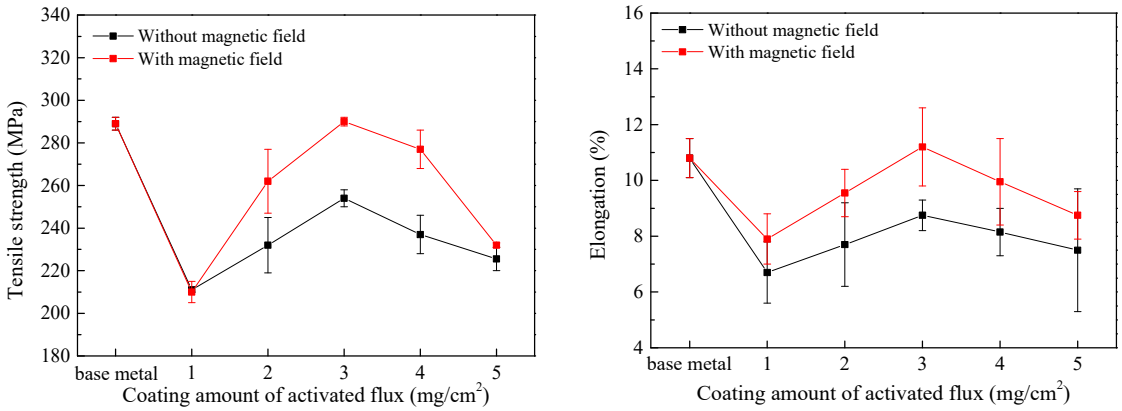

Figure 11. Tensile properties of welded joints and BM. (**a**) Tensile strength; (**b**) Elongation.

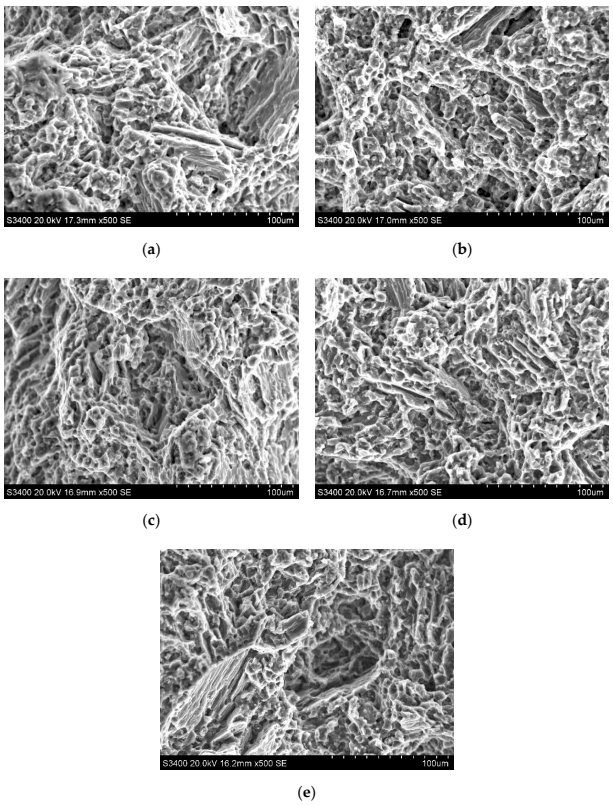

Figure 12. Fracture morphology under different amounts of activated flux (**a**) 1 mg/cm^2; (**b**) 2 mg/cm^2; (**c**) 3 mg/cm^2; (**d**) 4 mg/cm^2 (**e**) 5 mg/cm^2.

4. Conclusions

The effect of the longitudinal alternating magnetic field and TiO_2 flux on microstructure and mechanical properties of the AZ91 magnesium alloy welded joint was investigated. The conclusions are as follows:

(1) When the coating amount of activated flux is 3 mg/cm^2, the highest penetration of the welded joint is obtained, which is 141% of that without activated flux. Meanwhile, the mechanical properties reach the maximum, which is tensile strength of 292 MPa, elongation of 11.2%, and weld zone hardness of 75.6 HV.

(2) The combined effect of TiO_2 flux and magnetic field makes the liquid metal spiral downward, which makes the movement of the molten pool more violent and the solute redistribution more uniform, and it inhibits the emergence of preferential growth behavior.

(3) The combined effect of TiO_2 flux and magnetic field does not change the phase composition and the grain orientation of the weld metal, but can affect the grain size. The average grain size of weld metal under activated flux coating amount of 3 mg/cm^2 is 18.2% smaller than that under an activated flux coating amount of 1 mg/cm^2.

Author Contributions: G.Z. conceived and designed the experiments; X.L. performed the experiments and collected the data; Y.S. analyzed the data and drafted the paper. All authors have read and agreed to the published version of the manuscript.

Funding: The authors acknowledged the financial support by Liaoning Key Laboratories, Shenyang University of Technology (LJKZ0161).

Data Availability Statement: The data that supports the findings of the study is available from the corresponding author, G.Q.Z. and Y.H.S., upon reasonable request.

Conflicts of Interest: The authors declare no conflict of interest.

References

1. Viara, V.R.; Padmanaban, R.; Mohan, D.K.; Govindaraju, M. Research and development in the magnesium alloys for industrial and biomedical applications. *Met. Mater.* **2020**, *6*, 409–430.
2. Karakulak, E. A review: Past, present and future of grain refining of magnesium castings. *J. Magn. Alloy.* **2019**, *7*, 355–369. [CrossRef]
3. Subravel, V.; Padmanaban, G.; Balasubramanian, V. Effect of pulse frequency on tensile properties and microstructural characteristics of Gas Tungsten Arc welded AZ31B magnesium alloy. *Trans. Indian Inst. Met.* **2015**, *68*, 353–362. [CrossRef]
4. Pierpaolo, C.; Antonello, A.; Felice, R.; Nicola, P. Microstructural aspects in FSW and TIG welding of cast ZE41A magnesium alloy. *Metall. Mater. Trans. B* **2016**, *47*, 1340–1346.
5. Lu, C.F.; Li, Y.J.; Zhang, K.; Li, X.G. Effect of welding current on microstructure and properties of TIG welded EW75 magnesium alloy. *Mater. Sci. Forum* **2016**, *852*, 142–148. [CrossRef]
6. Wang, P.; Song, G. Pulsed MIG welding of AZ31B magnesium alloy. *Mater. Sci. Technol.* **2011**, *27*, 518–524.
7. Lechoslaw, T.; Andrzej, K.; Tomasz, P. Structure and mechanical properties of MIG welded butt-joints of magnesium alloys. *Weld. Int.* **2016**, *30*, 202–207.
8. Forcellese, A.; Martarelli, M.; Simoncini, M. Effect of process parameters on vertical forces and temperatures developed during friction stir welding of magnesium alloys. *Int. J. Adv. Manuf. Technol.* **2016**, *85*, 595–604. [CrossRef]
9. Wang, W.D.; Deng, D.A.; Mao, Z.T.; Tong, Y.G.; Ran, Y. Influence of tool rotation rates on temperature profiles and mechanical properties of friction stir welded AZ31 magnesium alloy. *Int. J. Adv. Manuf. Technol.* **2017**, *88*, 2191–2200. [CrossRef]
10. Xiao, L.; Liu, L.; Zhou, Y. Resistance-spot-welded AZ31 magnesium alloys: PartI. Dependence of fusion zone microstructure on second phase particles. *Metall. Mater. Trans. A* **2010**, *41*, 1511–1522. [CrossRef]
11. Manladan, S.M.; Yusof, F.; Ramesh, S.; Fadzil, M. A review on resistance spot welding of magnesium alloy. *Int. J. Adv. Manuf. Technol.* **2016**, *86*, 1805–1825. [CrossRef]
12. Kashaev, N.; Riekehr, S.; Horstmann, M. Fatigue, fatigue crack propagation and mechanical fracture behavior of laser beam-welded AZ31 magnesium sheets. *Mater. Sci. Forum.* **2014**, *783*, 2310–2315. [CrossRef]
13. Quazi, M.M.; Ishak, M.; Aiman, M.H.; Salleh, M.N.N. Microstructure, mechanical, and failure characteristics of laser-microwelded AZ31B Mg alloy optimized by response surface. *Int. J. Adv. Manuf. Technol.* **2018**, *99*, 985–1001.
14. Shyu, S.W.; Huang, H.Y.; Tsen, K.H.; Chou, C.P. Study of the performance of stainless steel A-TIG welds. *J. Mater. Eng. Perf.* **2008**, *17*, 193–201. [CrossRef]

15. Vasudevan, M. Effect of A-TIG welding process on the weld attributes of type 304LN and 316LN stainless steels. *J. Mater. Eng. Perf.* **2017**, *26*, 1325–1336. [CrossRef]
16. Vora, J.J.; Abhishek, K.; Srinivasan, S. Attaining optimized A-TIG welding parameters for carbon steels by advanced parameter-less optimization techniques: With experimental validation. *J. Braz. Soc. Mech. Sci.* **2019**, *42*, 261. [CrossRef]
17. Kumar, M.P.; Kanth, V.K.; Ramki, A.; Jagadish, K.E. Experimental investigation of active flux coatings on AA-6082 using A-TIG welding process. In *Recent Advances in Material Sciences*; Springer: Singapore, 2019; pp. 37–49.
18. Marya, M. Theoretical and experimental assessment of chloride effects in the A-TIG welding of magnesium. *Weld. World.* **2002**, *46*, 7–21. [CrossRef]
19. Zhang, Z.D.; Liu, L.M.; Shen, Y.; Wang, L. Activating flux for arc welding of magnesium alloy. *Chin. J. Nonferrous Met.* **2005**, *15*, 912–916.
20. Liu, L.M.; Zhang, Z.D.; Shen, Y.; Wang, L. Effects of activating fluxes on TIG welding penetration of magnesium alloy. *Acta metall. Sin.* **2006**, *42*, 399–404.
21. Huang, Y.; Fan, D.; Yang, P.; Lin, T. Effects of activating fluxes on AC A-TIG weld penetration of magnesium alloy. *Trans. China Weld. Inst.* **2007**, *28*, 41–44.
22. Zhang, Z.D.; Fan, F.Q. Study on effect of metal chlorides on penetration depth in A-TIG welding. *Trans. China Weld. Inst.* **2013**, *34*, 29–32.
23. Du, X.C.; Guo, S.L.; Dong, W.; Xu, X.D. Design and research on AZ31B alloy single surfactant for A-TIG welding. *Hot Work. Technol.* **2014**, *43*, 175–178.
24. Ma, X.; Zhang, Z.D.; Liu, L.M.; Liu, J.H. Effects of single and composite component oxides activating fluxes on A-TIG welding of magnesium alloy. *Trans. China Weld. Inst.* **2007**, *28*, 39–42.
25. Shen, J.; Zhai, D.J.; Liu, K.; Cao, Z.M. Effects of welding current on properties of A-TIG welded AZ31 magnesium alloy joints with TiO_2 coating. *Trans. Nonferrous Met. Soc. China* **2015**, *24*, 2507–2515. [CrossRef]
26. Qing, B.; Ying, F.C.; Zeng, C.Z.; Xie, J.C.; Shen, J. Microstructure and mechanical properties of TIG/A-TIG welded AZ61/ZK60 magnesium alloy joints. *Trans. Nonferrous Met. Soc.* **2019**, *29*, 1864–1872.
27. Shen, J.; Liu, K.; Li, S.Z. Effect of fluxes on distribution of SiC particles and microstructures and mechanical properties of nanoparticles strengthening A-TIG (NSA-TIG) welded magnesium alloy joints. *Sci. Technol. Weld. Join.* **2013**, *15*, 404–413. [CrossRef]
28. Qin, B.; Yin, F.C.; Xie, F.X.; Shen, J.; Xie, J.C.; Wu, D. Effects and distribution of TiC on the nanoparticle strengthening A-TIG welded AZ31 magnesium alloy joints. *Mater. Res. Express.* **2019**, *6*, 026543. [CrossRef]
29. Zhou, M.B.; Shen, J.; Hu, D.; Gao, R.H.; Li, S.Z. Effects of heat treatment on the activated flux TIG-welded AZ31 magnesium alloy joints. *Int. J. Adv. Manuf. Technol.* **2017**, *92*, 3983–3990. [CrossRef]
30. Demchenko, V.L.; Yurhenko, M.V. Structure and properties of the welded joints of single-type polyethylenes formed under the action of constant magnetic fields. *Mater. Sci.* **2017**, *53*, 186–193. [CrossRef]
31. Rui, L.; Xinjian, Y. Effect of axial magnetic field on TIG welding-brazing of AA6061 aluminum alloy to HSLA350 steel. *J. Mater. Res. Technol.* **2021**, *12*, 882–893.
32. Czernysz, W.; Ryzow, R.; Turyk, E. Influence of the electromagnetic effect in welding on the increase in the weld resistance to hot working. *Weld. Int.* **2004**, *18*, 257–262. [CrossRef]
33. Urusov, R.M.; Urusova, I.R. Mechanisms of the formation of an electric arc of a helical shape in an external axial magnetic field. *High Temp.* **2019**, *57*, 298–307. [CrossRef]
34. Su, Y.H.; Liu, Z.J.; Wang, Y.; Zhang, G.Q. Effect of magnetic field para-meters on microstructure and properties of welded joint of AZ31 magnesium alloy. *Trans. China Weld. Inst.* **2007**, *28*, 45–48.
35. Su, Y.H.; Jiang, H.W.; Qin, H.; Liu, Z.J. Forming characteristics, microstructure and properties of magnesium alloy during TIG welding under magnetic field. *Trans. China Weld. Inst.* **2013**, *34*, 85–88.
36. Su, Y.H.; Lin, J.L.; Jiang, H.W.; Liu, Z.J. Formability and microstructure of magnesium alloy welded by A-TIG under magnetic field. *Trans. China Weld. Inst.* **2013**, *34*, 13–16.
37. Su, Y.H.; Ai, X.Y.; Song, B.Q. Arc shape of magnetic field controlled A-TIG welding for AZ91 alloy and microstructure and properties welded joint. *J. Shenyang Univ. Technol.* **2018**, *40*, 505–510.